# Quantification of $^{11}$C-MADAM Binding to the Serotonin Transporter in the Human Brain

Johan Lundberg, MD[1]; Ikuo Odano, MD[2]; Hans Olsson, MD[1]; Christer Halldin, PhD[1]; and Lars Farde, MD[1]

[1]Department of Clinical Neuroscience, Section of Psychiatry, Karolinska Institutet, Stockholm, Sweden; and [2]Department of Sensory and Integrative Medicine, Division of Functional Imaging, Niigata University Graduate School of Medicine and Dental Sciences, Asahimachi-dori Niigata, Japan

$^{11}$C-N,N-Dimethyl-2-(2-amino-4-methylphenylthio)benzylamine ($^{11}$C-MADAM) is a newly synthesized radioligand with high selectivity and specificity for the serotonin transporter (5-HTT) in a monkey model. The purpose of this study in humans was to examine the suitability and potential of $^{11}$C-MADAM for quantitative PET studies of 5-HTT in applied clinical studies on the pathophysiology and treatment of neuropsychiatric disorders. **Methods:** PET examination was performed on each of 9 male subjects after intravenous injection of $^{11}$C-MADAM with high specific radioactivity. Radioactive metabolites in plasma were determined with high-performance liquid chromatography. A metabolite-corrected arterial input function was used in kinetic 2- and 3-compartment analyses. Cerebellum was used as the reference region in a cross-validation of 6 reference tissue approaches. **Results:** The highest radioactivity concentration was detected in the raphe nuclei, followed consecutively by the striatum, hippocampal complex, cingulate cortex, neocortex, and cerebellum. The time–activity curve for the fraction of unchanged $^{11}$C-MADAM in plasma was best described by a sigmoid function. After 50 min, the fraction was 40%. The labeled metabolites were more polar than the mother compound. The compartment model approaches converged, and could describe the time–activity curves in all regions. The total volume of distribution ($V_t$) was similar to the regional distribution volumes obtained by the linear graphic analysis. The binding potentials (BPs) for 6 different approaches yielded similar values in all regions but the raphe nuclei, where the 2 equilibrium methods provided lower values. **Conclusion:** The regional binding distribution of $^{11}$C-MADAM is consistent with postmortem data acquired with $^{3}$H-MADAM as well as with that of other reference ligands in vitro. The time–activity curves were well described by current major quantitative approaches. The suitability of the cerebellum as a reference region for nonspecific $^{11}$C-MADAM binding could be confirmed, thus paving the way for experimentally less demanding approaches, such as the simplified reference tissue model, for applied clinical studies.

**Key Words:** brain; humans; serotonin transporter; serotonin; PET

**J Nucl Med 2005; 46:1505–1515**

The serotonin transporter (5-HTT) is of central interest in the pathophysiology and treatment of psychiatric disorders such as anxiety and depression. This interest has been driven by early findings of decreased 5-HTT densities in suicide victims and in patients with major depression postmortem. Furthermore, the 5-HTT is the primary target for specific serotonin reuptake inhibitors (SSRIs), a group of drugs widely prescribed for the treatment of mood and anxiety disorders (1).

Studies on the pathophysiology and pharmacology of the 5-HTT in humans in vivo has for several years been hampered by the lack of suitable radioligands for PET and SPECT. Of radioligands developed earlier, the diphenyl sulfide derivative 3-amino-4-(2-dimethylaminomethylphenylsulfanyl)-benzonitrile ($^{11}$C-DASB) (2) has shown the most promising characteristics (3,4).

We have recently reported on N,N-dimethyl-2-(2-amino-4-methylphenylthio)benzylamine (MADAM), a new radioligand with high selectivity and specificity for the 5-HTT (5,6). Initial characterization of $^{11}$C-MADAM in monkey brain has shown high specific binding in the brainstem, thalamus, and striatum and lower binding in cortical regions (7). The rank order of specific binding was in agreement with that of human postmortem data (8–11).

The aim of the present PET study on 9 healthy subjects was to examine the potential of $^{11}$C-MADAM for quantitative studies of 5-HTT in the human brain. The standard 2- and 3-compartment models (2CM, 3CM) and 6 derived approaches were used and compared in an attempt to select the most appropriate method for applied quantitative studies. The prospects for quantification of 5-HTT binding in the hippocampal complex and the raphe nuclei were given particular attention.

## MATERIALS AND METHODS

### Subjects and Design

The study was approved by the Ethics and the Radiation Safety Committees of the Karolinska Hospital. Nine male subjects, 22–55 y old, participated after giving informed consent. All subjects were healthy according to history, psychiatric interview, physical examination, blood and urine analysis, and MRI of the brain. They did not use any medication and they were all nonsmokers. Each subject was examined once with PET and $^{11}$C-MADAM.

## MRI and Head Fixation System

The MRI system used for all subjects was a Signa, 1.5 T (GE Healthcare). T2-weighted and proton density images (156 × 1.0 mm slices) were obtained. To allow the same head positioning in the 2 imaging modalities, a head fixation system with an individual plaster helmet was used both in the PET and the MRI measurements (12).

## Radiochemistry

[11]C-MADAM (for chemical structure, see (13)) was obtained by methylation of 2-((2-((dimethylamino)methyl)phenyl)thio)-5-iodophenylamine (ADAM) using ^{11}C-methyl iodide, as described previously (13). Between 282 and 318 MBq were injected intravenously. The specific radioactivity of the radioligand injected varied between 5.4 and 78 GBq/mmol, corresponding to an injected mass of 0.74–11.9 μg.

## PET Experimental Procedure

The PET system used was an ECAT Exact HR 47 (Siemens), which was run in the 3-dimensional mode (14). The in-plane and axial resolution is about 3.8 and 4.0 mm, respectively, full width at half maximum. The reconstructed volume was displayed as 47 sections with a center-to-center distance of 3.125 mm.

In each PET measurement, the subject was placed recumbent with his head in the PET system. One cannula was inserted into the left brachial artery and another was inserted into the right antecubital vein. Sterile physiologic phosphate buffer solution (pH 7.4) containing ^{11}C-MADAM was injected as a bolus over 2 s into the right antecubital vein. The cannula was then immediately flushed with 10 mL saline.

Brain radioactivity was measured in a series of consecutive time frames for 93 min. The frame sequence consisted of three 1-min frames, four 3-min frames, and thirteen 6-min frames. However, for one subject, the measurement lasted for 87 min, resulting in a reduction of one 6-min frame compared with the original frame sequence.

## Arterial Blood Sampling

To obtain the arterial input function, an automated blood sampling system was used during the first 5 min of each PET measurement (15). After the first 5 min, arterial blood samples (2 mL) were taken manually at the midpoint of each frame until the end of the measurement (16).

## Determination of Radioactive Metabolites in Plasma

The fractions of plasma radioactivity corresponding to unchanged ^{11}C-MADAM and metabolites were determined as has been described previously for other radioligands (17). In brief, arterial plasma samples (2 mL taken at 4, 10, 20, 30, 40, and 50 min) were deproteinized with acetonitrile and analyzed by gradient high-performance liquid chromatography high-performance liquid chromatography (HPLC). Unlabeled MADAM was used as a reference to provide retention times for possible labeled metabolites in plasma.

## Regions of Interest (ROIs)

ROIs were defined according to anatomic boundaries for frontal cortex, cingulate cortex, hippocampal complex, putamen, raphe nuclei, and cerebellum. All ROIs except for the raphe nuclei were delineated in 3 consecutive sections on the MR images and transferred to the corresponding reconstructed PET images. On MR images the raphe nuclei cannot be differentiated from surrounding tissue. Therefore, these ROIs were delineated directly on the PET images in 3–5 sections, as a standardized circular ROI of 6 mm was applied.

## Time–Activity Curves

To obtain the radioactivity concentration for each region, data for all sectional ROIs of that region were pooled. Regional radioactivity was calculated for each frame, corrected for decay, and plotted versus time, thus providing regional time–activity curves.

Before entering quantitative analysis, the time–activity curves were corrected for the effect of radioactivity in the cerebral blood volume (CBV) using the following equation:

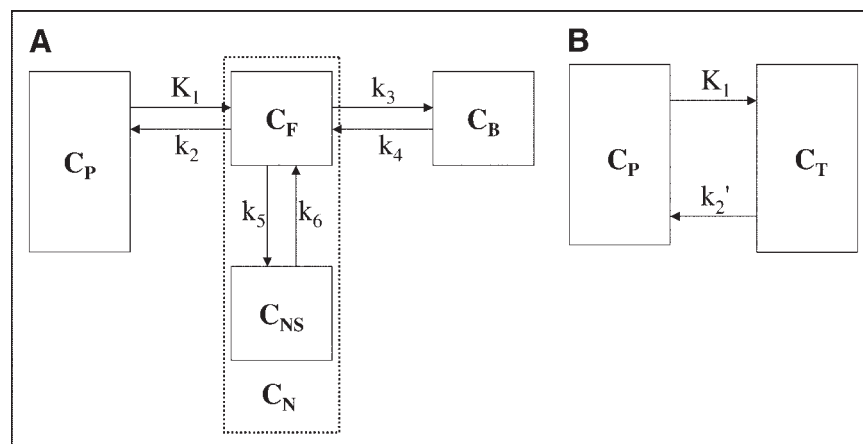$$C_{pet}(t) = C_T(t) + \alpha \cdot C_a(t), \qquad \text{Eq. 1}$$

where $C_{pet}(t)$ represents the radioactivity measured by the PET system, $a$ represents the CBV, and $C_a(t)$ is the time curve for arterial whole blood. $a$ was set to 0.04, the average blood volume in gray matter (16,18,19).

## Quantitative Analyses

The 2CM, 3CM, and 6 derived approaches were compared to select the most appropriate method for applied quantitative studies. The binding potential (BP) was the parameter compared.

*Kinetic Compartment Analyses.* The data were analyzed using compartment models. The general configuration is a conventional 4-compartment model with 6 rate constants (K₁, k₂, k₃, k₄, k₅, k₆; Fig. 1A). $K_1$ (mL · mL$^{-1}$ · min$^{-1}$) and $k_2$ (min$^{-1}$) correspond to the influx and efflux rates for radioligand diffusion through the blood–brain barrier, respectively. The rate constants $k_3$ (min$^{-1}$) and $k_4$ (min$^{-1}$) correspond to the rates for radioligand transfer between



**FIGURE 1.** The 3- and 4-compartment model. The 4 compartments correspond to the radioactivity concentration of unchanged radioligand in plasma ($C_P$), unbound radioligand in brain ($C_F$), nonspecifically bound radioligand in brain ($C_{NS}$), and radioligand specifically bound to receptors ($C_B$). With the assumption that $C_F$ and $C_{NS}$ rapidly coalesce, they can be substituted with one compartment representing nondisplaceable radioligand ($C_N$, dotted line) (A). In the 2-compartment model, $C_B$ and $C_N$ are substituted by one tissue compartment ($C_T$) (B).

unbound radioligand in brain ($C_F$, radioactivity concentration of free (unbound) radioligand in brain) and radioligand specifically bound to receptors ($C_B$, radioactivity concentration of radioligand specifically bound to receptors). Radioligand transfer between $C_F$ and nonspecifically bound radioligand in brain ($C_{NS}$, radioactivity concentration of nonspecifically bound radioligand) is described by $k_5$ and $k_6$ (both with the dimension $min^{-1}$). All 4 compartments were assumed homogeneous in concentration and all concentrations have the dimension 37 Bq/mL (nCi/mL).

A common assumption is that the 2 compartments $C_F$ and $C_{NS}$ equilibrate rapidly, thus forming one effective compartment [20], which corresponds to nondisplaceable radioligand in brain ($C_N$). Assuming that $C_F$ and $C_{NS}$ equilibrate rapidly, the model can be simplified into 3 compartments and 4 rate constants (Fig. 1A). This model was used to describe the time–activity curves for ^{11}C-MADAM. The radioactivity concentration in plasma was not corrected for plasma protein binding.

On the basis of this model, the following differential equations can be expressed:

$$dC_N(t)/dt = K_1C_P(t) - (k_2 + k_3)C_N(t) + k_4C_B(t). \quad \text{Eq. 2}$$

$$dC_B(t)/dt = k_3C_N(t) - k_4C_B(t). \quad \text{Eq. 3}$$

$$C_T(t) = C_N(t) + C_B(t), \quad \text{Eq. 4}$$

where $C_T(t)$ is the radioactivity concentration in brain, corrected for CBV.

The 2CM (Fig. 1B) is a simplification of the 3CM based on the assumption that all of the compartments, $C_F$, $C_{NS}$, and $C_B$, equilibrate rapidly to form one effective compartment, $C_T$. The 2CM was used as an alternative approach to describe the time–activity curves for ^{11}C-MADAM [19]. Here $K_1$ corresponds to the influx rate of radioligand diffusion through the blood–brain barrier. The rate constant $k_2'$ corresponds to the efflux rate, and its relation to $k_2$, $k_3$, and $k_4$ of the 3CM is given by Equation 5:

$$k_2' = k_2/(1 + k_3/k_4). \quad \text{Eq. 5}$$

In the 3CM analysis the 4 rate constants were determined by curve fitting in a nonlinear least-squares minimization procedure using the Simplex algorithm [21] with constraints for $K_1$ being restricted between 0 and 99.9 and for $k_2$, $k_3$, and $k_4$ between 0 and 9.9. The initial values for $K_1$, $k_2$, $k_3$, and $k_4$ were 0.5, 0.5, 2.0, and 0.5, respectively, and the local minimum of the sum of the squared residuals was determined by an iterative procedure.

*Calculation of BP.* Classical receptor binding parameters, such as receptor density ($B_{max}$) and affinity ($K_d$), cannot be differentiated on the basis of one PET measurement with high specific radioactivity [22]. The ratio $B_{max}/K_d$ is often referred to as the BP. It corresponds to the ratio $k_3/k_4$ in the kinetic analysis. In the present study, BPs calculated directly from $k_3$ and $k_4$ of the 3-compartment analysis are referred to as $BP_{Direct(1)}$.

A variant of a 3-compartment analysis, 3CM(2), was applied with the assumption that $C_N$ is identical among all ROIs. In this approach, the $K_1/k_2$ ratio was fixed to the ratio for the reference region obtained with the 2CM. The BPs calculated from the thereby acquired $k_3$ and $k_4$ values are referred to as $BP_{Direct(2)}$.

[11]C-MADAM binding was also expressed using the concept of the total volume of distribution, which for the 3CM is defined as:

$$V_t = (K_1/k_2)(1 + k_3/k_4). \quad \text{Eq. 6}$$

The ratio of $V_t$ in the ROI ($V_t^{ROI}$) and the $V_t$ in the reference region ($V_t^{REF}$) was entered into the following equation to calculate the $BP_{Indirect}$:

$$BP_{Indirect} = (V_t^{ROI}/V_t^{REF}) - 1. \quad \text{Eq. 7}$$

The BP was also calculated by means of the simplified reference tissue model ($BP_{SRTM}$) and by the linear graphic analysis for reversible ligand binding to receptors developed by Logan et al., as described in the literature [23,24]. The linear graphic analysis provides the regional distribution volume (DV) from which the BP can be calculated ($BP_{Logan}$).

The ratio $C_B/C_N$ is equal to the BP when $dC_B/dt = 0$. In this moment—that is, the time of transient equilibrium—the number of molecules associating with the receptors is equal to the number dissociating [16,25,26]. This is the basis for the transient equilibrium approach ($BP_{EqA}$ and $BP_{EqB}$), which also was used to determine the BP as described in the literature. The BP is referred to as $BP_{EqA}$. A flat shape of $C_B(t)$ may make it difficult to define time of peak equilibrium with high reliability. As an alternative approach, the area under the time–activity curve for $C_B(t)$ and $C_N(t)$ during the time interval 57–93 min was used to calculate $BP_{EqB}$.

### Cerebellum as Reference Region
The cerebellum is a region with very low density of 5-HTT in the human brain in vitro [8,9,11]. In a pretreatment experiment with citalopram, 5 mg/kg, in monkey, radioactivity in all examined brain regions was reduced to the level of the cerebellum [7,27]. Thus, there is in vitro and in vivo support for a role of the cerebellum as the reference region in calculations of BP.

### Statistics
Three statistical methods were used to compare the 2 models: the Akaike information criterion (AIC) [28], the Schwarz criterion [29], and F statistics on the squared differences between obtained data and model output [30].

## RESULTS

After injection of ^{11}C-MADAM with high specific activity, radioactivity appeared rapidly in the brain (Fig. 2). The highest radioactivity concentration was found in the raphe nuclei, followed by the putamen, hippocampal complex, cingulate cortex, and frontal cortex. Radioactivity was lowest in the cerebellum (Fig. 3).

The fraction of radioactivity in plasma representing unchanged ^{11}C-MADAM was measured by HPLC. There was a decrease with time and, at 50 min after ^{11}C-MADAM injection, the fraction was about 40% (Fig. 4). At samples drawn after 50 min, the signal-to-noise ratio was not sufficiently high to accurately determine the fractions. The labeled metabolites revealed by the HPLC were more polar than the mother compound.

The plasma radioactivity curves were corrected for radioligand metabolism and plotted versus time (Fig. 3). After an immediate increase, there was a rapid decrease of radioactivity during the first 5 min after radioligand injection. After this time, the decrease continued throughout the experiment but at a slower rate.

In the kinetic analysis, the 2CM and 3CM converged and could describe all regional time–activity curves (Fig. 5).
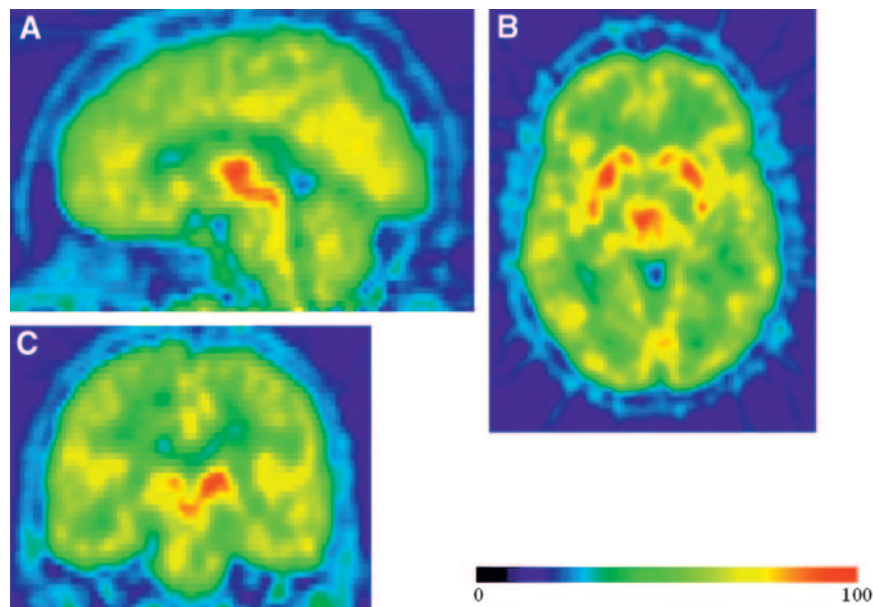
**FIGURE 2.** Summation image based on data from frames 6–20 showing regional radioactivity after intravenous injection of $^{11}$C-MADAM. Projections are, clockwise from top left, sagittal (A), transaxial (B), and coronal (C).

The estimated rate constants are given in Table 1. In 16 of the 63 ROIs studied, the 3CM(1) was statistically superior in describing the time–activity curve, in terms of F statistics as well as the Akaike and Schwarz criteria. The 16 cases in which the 3CM(1) was statistically superior were distrib-uted over all regions including the cerebellum, but not the raphe. A detailed presentation of data obtained for the cerebellum is given in Table 2.

In the second 3-compartment approach, 3CM(2), the ratio of $K_1/k_2$ was constrained and defined by the cerebellum.
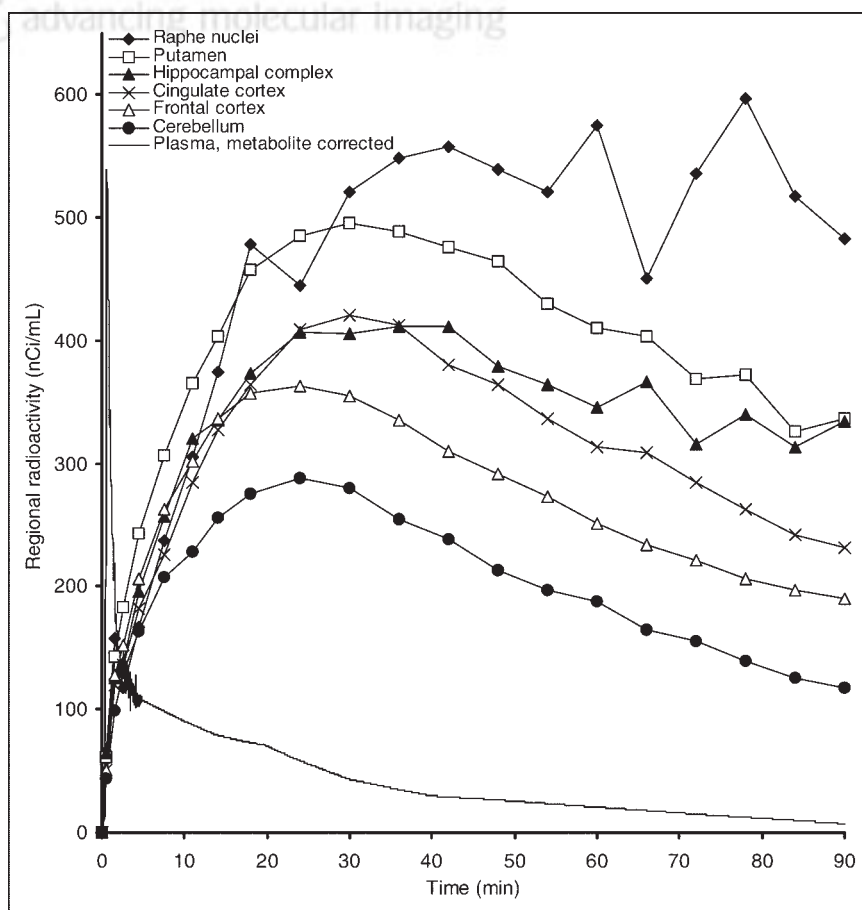


**FIGURE 3.** Time–activity curves of ROIs and of plasma input function in one sub-ject.
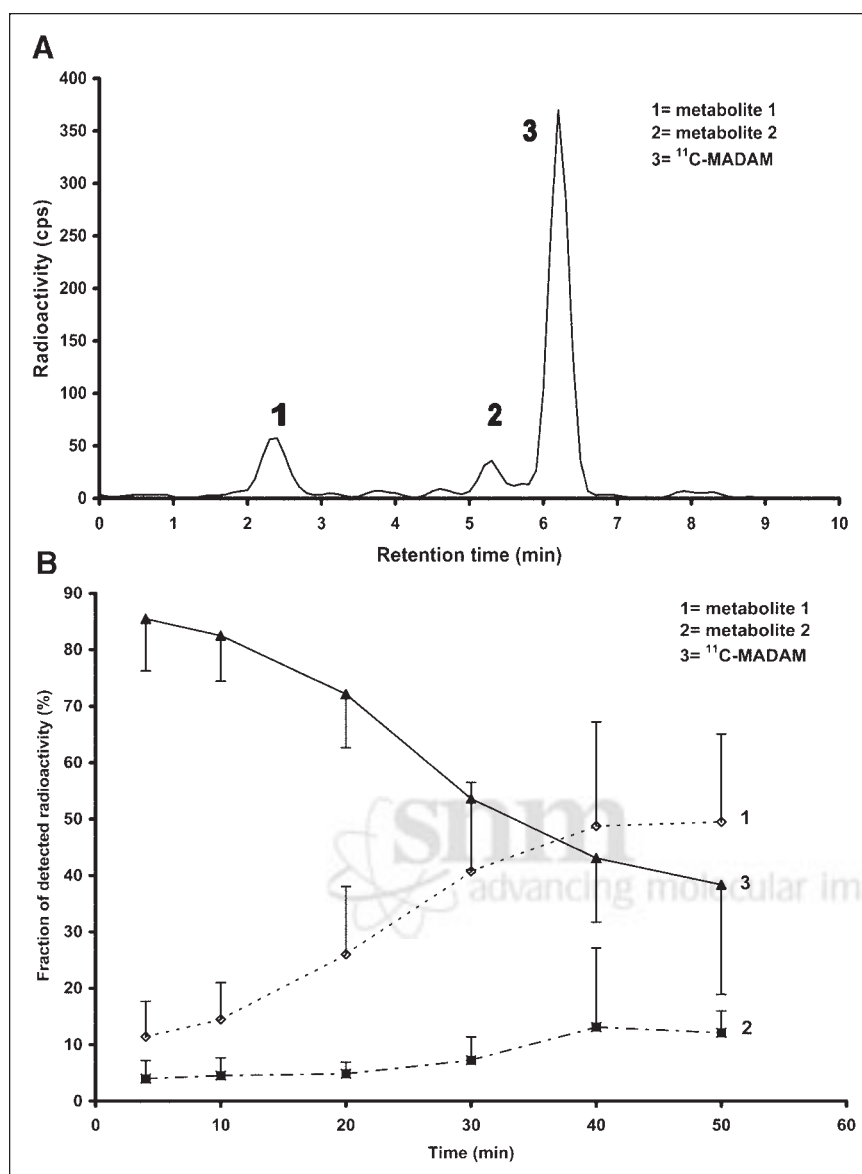
**FIGURE 4.** (A) Labeled metabolites detected by HPLC (1 and 2) were more polar than the mother compound ^{11}C-MADAM (3) (based on 4-min sample from one subject). (B) Fraction of detected radioactivity in plasma: 1, 2 and 3 correspond to the 3 peaks in HPLC (mean ± SD, $n = 9$).

This approach was statistically superior to the 2CM in 16 of the 54 regions (not applicable for the cerebellum).

The total volume of distribution, $V_t$, obtained by the 3CM(1) and the 3CM(2) showed a significant correlation within all regions (Pearson correlation coefficients, 0.988–0.999; $P < 0.001$, 2-tailed; Table 3). In the linear graphic analysis, a linear phase was observed for all regions (Fig. 6). The regional distribution volumes (DV) obtained by the linear graphic analysis were correlated with the $V_t$ values obtained by the compartment analyses (Pearson correlation coefficients, 0.960–0.999 within all regions; $P < 0.001$; 2-tailed; Table 3).

The BP was calculated for the 7 approaches (Table 4). In all analyzed regions, the $BP_{Direct(1)}$ gave 2–6 times higher values than the other methods. For several regions, the SD exceeded the mean value. All other methods yielded similar regional BP values, with the exception of the raphe region, where the equilibrium approaches provided low values when compared with other methods (Table 4).

## DISCUSSION

After intravenous injection of ^{11}C-MADAM, there was a marked uptake in all neocortical regions, the striatum, and the raphe nuclei (Figs. 2 and 3). The PET system provided a good signal-to-noise ratio in all regions examined, with the highest ratio in the raphe, where it was higher than 3, and the lowest ratio in the frontal cortex, where it was about 2. The rank order is in good agreement with postmortem studies of radioligand binding to 5-HTT in the human brain (8–11) (Table 5), including a recent study using ^{3}H-MADAM (6). In concurrence with previous characterization of ^{11}C-MADAM in a primate model (7,27), this re-
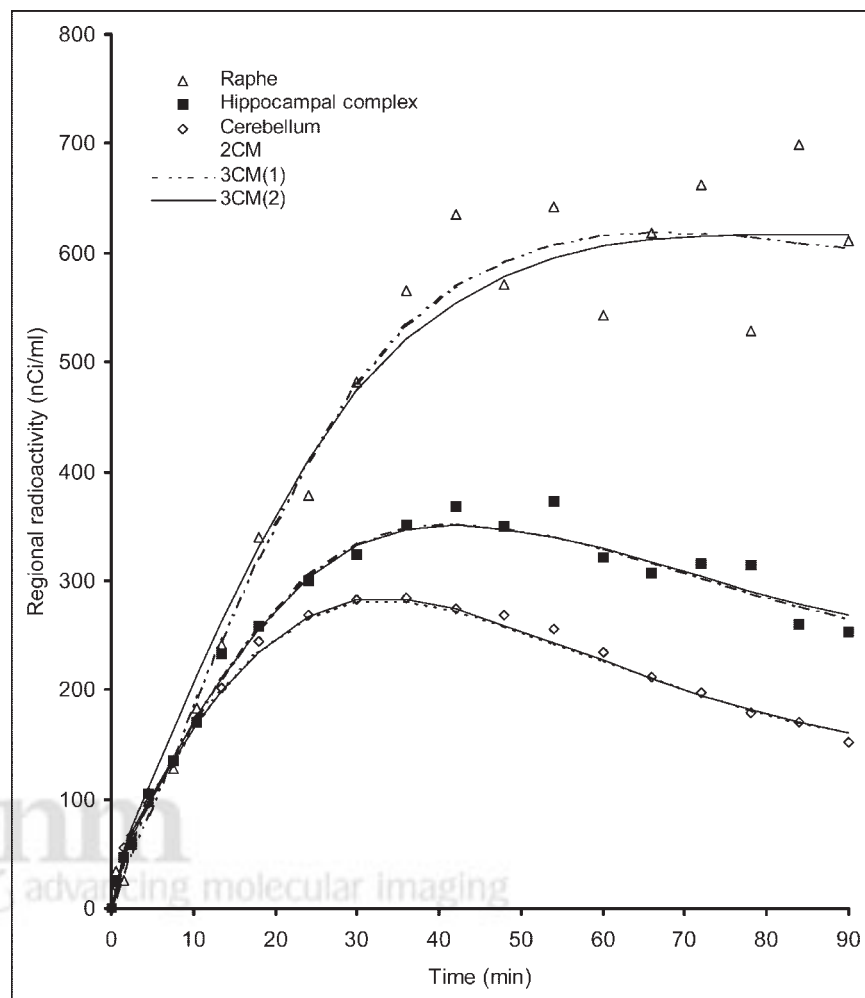
**FIGURE 5.** Experimental values of regional activity and corresponding fitted curves as obtained by the 2CM, the unconstrained 3CM (3CM(1)), and the 3CM with the $K_1/k_2$ ratio given by that of cerebellum (3CM(2)).

gional distribution provides support that ^{11}C-MADAM binds specifically to 5-HTT in the human brain in vivo.

The time–activity curve for the fraction of unchanged ^{11}C-MADAM in plasma was best described by a sigmoid function (Fig. 4). Similar observations have been made previously for other radioligands with affinity for 5-HTT and may be explained by high initial uptake of radioligand in lung tissue (*31*). Of particular interest is that affinity for lung tissue has been described in rodents for the structurally akin radioligand ^{123}I-ADAM (*32*). A consequence of high initial uptake in lung tissue is a low exposure of radioligand to metabolic enzymes, which thus may explain the low initial metabolic rate. The uptake in lung may also explain the relatively slow distribution of ^{11}C-MADAM to brain (Fig. 3), when compared with other radioligands, such as ^{11}C-raclopride, ^{11}C-SCH 23390, and ^{11}C-WAY 100635 (*33,34*).

Reversibility of ^{11}C-MADAM binding has been demonstrated in primates by a displacement experiment using citalopram (*27*). In the present study in humans, reversibility is supported by $k_4$ values above zero and by the linear graphic analysis since the latter part of the curves can be described by a linear function and the slopes do not approach infinity (Fig. 6).

Cerebellum was used as the reference region because this region has been demonstrated to have negligible 5-HTT density in vitro (Table 5). The validity of $C_N$ for cerebellum as an index for $C_N$ in other regions has been confirmed by experiments in nonhuman primates showing that the time–activity curves for all regions with specific ^{11}C-MADAM binding decreased to the level of the cerebellum after pretreatment with citalopram (5 mg/kg) (*7,27*).

For the cerebellum, the time–activity curves could be described by the 3CM(1) and, in this respect, there was a high degree of consistency between individuals (Fig. 5; Table 2). The 3CM(1) was statistically superior to the 2CM in only 2 of the 9 subjects (Table 2). This observation may support the model assumption of a rapid equilibrium between the $C_{NS}$ and $C_F$ in the cerebellum—that is, for a reference region devoid of specific binding, a collapse of 3 compartments into 2 (*20*). Clearly, the compartment model analysis does not give support for the existence of kinetically distinguishable nonspecific binding, as has been shown for other radioligands, such as ^{11}C-WAY 100635 (*34*).

Importantly, despite the observations regarding the validity of the cerebellum as a reference region, calculation of regional $C_N$ based on the 3CM(1) data resulted in a curve

## TABLE 1
### Rate Constants for Compartment Models

| Model | Region | $K_1$ | $k_2$ | $k_3$ | $k_4$ |
|---|---|---|---|---|---|
| 2CM* | Frontal cortex | 0.31 ± 0.09 | 0.04 ± 0.01 | na | na |
| | Cingulate cortex | 0.28 ± 0.05 | 0.03 ± 0.01 | na | na |
| | Hippocampal complex | 0.28 ± 0.06 | 0.02 ± 0.01 | na | na |
| | Putamen | 0.33 ± 0.09 | 0.02 ± 0.01 | na | na |
| | Raphe nuclei | 0.30 ± 0.06 | 0.01 ± 0.01 | na | na |
| | Cerebellum | 0.26 ± 0.07 | 0.04 ± 0.01 | na | na |
| 3CM(1) | Frontal cortex | 0.60 ± 0.25 | 0.30 ± 0.19 | 1.11 ± 0.76 | 0.45 ± 0.45 |
| | Cingulate cortex | 0.46 ± 0.19 | 0.18 ± 0.13 | 1.26 ± 0.76 | 0.48 ± 0.42 |
| | Hippocampal complex | 0.52 ± 0.19 | 0.23 ± 0.16 | 1.11 ± 0.89 | 0.44 ± 0.45 |
| | Putamen | 0.78 ± 0.42 | 0.34 ± 0.30 | 1.29 ± 0.79 | 0.49 ± 0.44 |
| | Raphe nuclei | 0.62 ± 0.53 | 0.39 ± 0.70 | 0.70 ± 0.84 | 0.16 ± 0.24 |
| | Cerebellum | 0.55 ± 0.20 | 0.33 ± 0.19 | 1.23 ± 0.71 | 0.64 ± 0.44 |
| 3CM(2) | Frontal cortex | 0.46 ± 0.19 | 0.08 ± 0.04 | 0.38 ± 0.35 | 0.86 ± 0.87 |
| | Cingulate cortex | 0.44 ± 0.15 | 0.08 ± 0.03 | 0.75 ± 0.53 | 1.00 ± 0.66 |
| | Hippocampal complex | 0.81 ± 0.50 | 0.14 ± 0.09 | 1.30 ± 0.98 | 1.30 ± 0.90 |
| | Putamen | 0.79 ± 0.42 | 0.14 ± 0.07 | 1.48 ± 0.86 | 1.13 ± 0.78 |
| | Raphe nuclei | 0.40 ± 0.08 | 0.07 ± 0.02 | 0.83 ± 0.78 | 0.97 ± 0.51 |
| | Cerebellum | na | na | na | 0.78 ± 0.59 |

*For 2CM, $k_2'$ values are presented in the $k_2$ column.

na = not applicable.

Values are presented as mean ± SD ($n = 9$).

clearly under the level of the cerebellum time–activity curve (Fig. 7A). This suggests that, although the 3CM(1) does converge, it does not deliver reliable rate constants. As given by the model approach, 3CM(2) provided rate con-stants that describe $C_N(t)$ in accordance with the cerebellum curve (Fig. 7B). This approach gave similar BP values as the 5 other methods, which depends on the cerebellum as the reference tissue.

## TABLE 2
### Comparison of 2CM and 3CM in Cerebellum

| Subject | Model | $K_1$ (mL · mL$^{-1}$ · min$^{-1}$) | $k_2$ (min$^{-1}$) | $K_5$ (min$^{-1}$) | $K_6$ (min$^{-1}$) | RSS | AIC | SC | F statistics ($n = 9$) |
|---|---|---|---|---|---|---|---|---|---|
| 1 | 2CM | 0.18 | 0.04 | | | 871 | 139 | 141 | |
| | 3CM(1) | 0.71 | 0.52 | 2.02 | 0.91 | 879 | 144 | 148 | ns |
| 2 | 2CM | 0.30 | 0.05 | | | 438 | 126 | 128 | |
| | 3CM(1) | 0.71 | 0.25 | 1.68 | 1.30 | 500 | 132 | 136 | ns |
| 3 | 2CM | 0.21 | 0.04 | | | 642 | 133 | 135 | |
| | 3CM(1) | 0.38 | 0.17 | 1.21 | 0.93 | 667 | 138 | 142 | ns |
| 4 | 2CM | 0.19 | 0.04 | | | 560 | 131 | 133 | |
| | 3CM(1) | 0.39 | 0.31 | 1.69 | 0.69 | 576 | 135 | 139 | ns |
| 5 | 2CM | 0.23 | 0.04 | | | 2,827 | 163 | 165 | |
| | 3CM(1) | 0.50 | 0.69 | 0.48 | 0.08 | 1,932 | 159 | 163 | $P < 0.005$ |
| 6 | 2CM | 0.25 | 0.04 | | | 614 | 132 | 134 | |
| | 3CM(1) | 0.35 | 0.22 | 0.57 | 0.20 | 618 | 137 | 141 | ns |
| 7 | 2CM | 0.32 | 0.04 | | | 641 | 133 | 135 | |
| | 3CM(1) | 0.75 | 0.29 | 1.86 | 0.91 | 694 | 139 | 143 | ns |
| 8 | 2CM | 0.40 | 0.07 | | | 1,989 | 156 | 158 | |
| | 3CM(1) | 0.85 | 0.43 | 1.56 | 0.74 | 1,961 | 160 | 164 | ns |
| 9 | 2CM | 0.28 | 0.04 | | | 1,109 | 137 | 139 | |
| | 3CM(1) | 0.31 | 0.05 | 0.01 | 0.04 | 455 | 124 | 128 | $P < 0.0001$ |
| Mean ± SD | 2CM | 0.26 ± 0.07 | 0.05 ± 0.01 | | | | | | |
| | 3CM(1) | 0.55 ± 0.20 | 0.33 ± 0.19 | 1.23 ± 0.71 | 0.65 ± 0.44 | | | | |

RSS = residual sum of squares; AIC = Akaike information criteria; SC = Schwartz criteria; ns = not significant.

**TABLE 3**
Total Volume of Distribution, $V_t$, Obtained by 3CM(1),
3CM(2), and Distribution Volume Obtained by
Linear Graphic Analysis, DV

| Region | $V_{t\ 3CM(1)}$ | $V_{t\ 3CM(2)}$ | DV |
|---|---|---|---|
| Frontal cortex | 8.5 ± 1.5 | 8.5 ± 1.5 | 8.5 ± 1.5 |
| Cingulate cortex | 10.2 ± 1.8 | 10.8 ± 2.1 | 10.0 ± 1.8 |
| Hippocampal complex | 11.8 ± 2.2 | 11.8 ± 2.1 | 11.8 ± 2.4 |
| Putamen | 14.3 ± 3.1 | 14.5 ± 2.9 | 14.2 ± 3.1 |
| Raphe nuclei | 33.8 ± 15.7 | 33.6 ± 15.8 | 29.2 ± 10.6 |
| Cerebellum | 5.9 ± 1.2 | na | 5.8 ± 1.2 |

na = not applicable.
Values are presented as mean ± SD ($n = 9$).

Macrosystem parameters, such as the distribution volume ($K_1/k_2[1 + k_3/k_4]$), have been acknowledged as being more reliable than individual parameters, such as single rate constants (35). Notably, the distribution volumes based on 3CM(1) and 3CM(2) are very similar to the ones calculated using the linear graphic method (Table 3). The previously mentioned initial accumulation in lung tissue and slow redistribution to brain may yield an unfavorable input function and be a reason for the failure to obtain reliable individual rate constants with 3CM(1). This suggestion is supported by the literature reporting a similar problem in work with other radioligands also belonging to the diphenyl sulfide derivative class, which, accordingly, might share affinity for lung tissue (2,36–38).

The coefficient of variation was highest for the raphe nuclei and, in some approaches, the hippocampal complex (Table 4). These are small regions that also had the highest level of noise (defined by the squared differences between the obtained data and the 3CM(2) model output). Partial-volume effect (PVE) correction was not applied in this study, partly due to the relative homogeneity of the material examined and partly due to the particular attention given to the raphe nuclei, and because it is not possible to define on the MR images, it is not available to PVE correction. Still, because the raphe nuclei is of key interest for the mechanism of action of SSRIs and
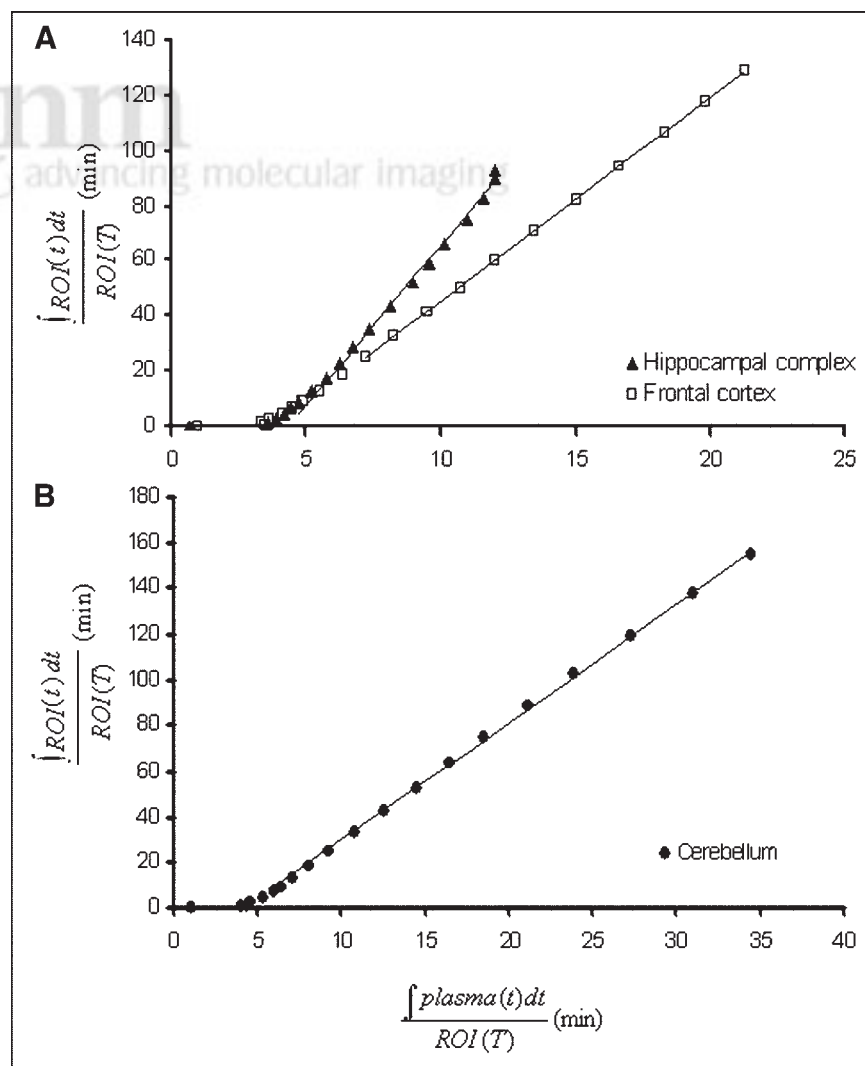


**FIGURE 6.** Linear graphic analyses of ^{11}C-MADAM binding in hippocampal complex and frontal cortex (A) and cerebellum (B). Slope of linear phase corresponds to the DV.

**TABLE 4**
Comparison of BPs Produced with 7 Different Approaches

| Method | Region | | | | | | | | | | | | |
| --- | --- | --- | --- | --- | --- | --- | --- | --- | --- | --- | --- | --- | --- |
| | Frontal cortex | | Cingulate cortex | | Hippocampal complex | | Putamen | | Raphe nuclei | | Cerebellum | |
| $BP_{Direct(1)}$ | $3.2 \pm 2.0$ | 64 | $3.3 \pm 1.7$ | 52 | $4.7 \pm 6.0$ | 127 | $4.4 \pm 4.3$ | 97 | $10.9 \pm 14.6$ | 134 | $2.3 \pm 1.7$ | 73 |
| $BP_{Direct(2)}$ | $0.5 \pm 0.1$ | 20 | $0.8 \pm 0.2$ | 28 | $1.0 \pm 0.2$ | 24 | $1.5 \pm 0.3$ | 20 | $4.6 \pm 1.9$ | 41 | na | |
| $BP_{Indirect}$ | $0.4 \pm 0.1$ | 22 | $0.7 \pm 0.2$ | 27 | $1.0 \pm 0.2$ | 24 | $1.4 \pm 0.3$ | 20 | $4.6 \pm 1.8$ | 39 | na | |
| $BP_{Logan}$ | $0.5 \pm 0.1$ | 20 | $0.7 \pm 0.2$ | 27 | $1.0 \pm 0.2$ | 21 | $1.4 \pm 0.3$ | 19 | $4.1 \pm 1.2$ | 28 | na | |
| $BP_{SRTM}$ | $0.6 \pm 0.2$ | 31 | $0.7 \pm 0.1$ | 20 | $1.2 \pm 0.5$ | 43 | $1.4 \pm 0.2$ | 15 | $4.0 \pm 0.8$ | 20 | na | |
| $BP_{EqA}$ | $0.4 \pm 0.1$ | 27 | $0.7 \pm 0.1$ | 16 | $1.2 \pm 0.4$ | 35 | $1.3 \pm 0.2$ | 15 | $3.6 \pm 0.5$ | 14 | na | |
| $BP_{EqB}$ | $0.5 \pm 0.1$ | 19 | $0.8 \pm 0.2$ | 19 | $1.0 \pm 0.2$ | 19 | $1.5 \pm 0.3$ | 19 | $3.0 \pm 0.4$ | 15 | na | |

na = not applicable.
$BP_{Direct(1)} = k_3/k_4$. $BP_{Direct(2)} = k_3/k_4$; $K_1/k_2$ given by cerebellum.
$BP_{Indirect} = (V_{t\ 3CM(1)\ ROI}/V_{t\ 3CM(1)\ cerebellum}) - 1$.
All values are mean $\pm$ SD coefficient of variation (%) ($n = 9$).

because the hippocampal complex may have a role in mood disorder, the relatively poor reliability of 5-HTT quantification in these regions has to be taken in account when comparing individual data or small samples.

An analysis based on 3CM(2) with an arterial input function provides a full set of parameters. Nevertheless, in applied studies a simple protocol independent of arterial blood sampling offers practical advantages. Interestingly, several approaches independent of arterial blood sampling gave BP values in accordance with 3CM(2) (Table 4). Among these, the SRTM may be the most advantageous, as it is the only reference method that considers the entire time–activity curve. This is a feature of special importance when analyzing regions with a late equilibrium, such as the raphe nuclei. Thus, the SRTM may be advantageous for clinical studies on regional 5-HTT binding in the human brain.

[11]C-MADAM belongs to the group of diphenyl sulfide derivatives, as does ^{11}C-DASB, a ligand already applied for studies on 5-HTT occupancy (2,3). This class of molecules has clearly marked an opening in the quest for putative radioligands for quantification of 5-HTT in human brain using PET. One example of this advancement is the signal-to-noise-ratio that has been reported by Frankle et al. to be higher for ^{11}C-DASB than for the previously rather widely used 5-HTT radioligand ^{11}C-McN 5652 (39). Interestingly, a comparison of data from the present study with those of Frankle et al. (39) indicates even higher signal-to-noise-ratios for ^{11}C-MADAM: $BP_{Indirect}$ (based on mean values) is 2–3 times higher in most regions when compared with ^{11}C-DASB. The total volume of distribution in cerebellum, $5.9 \pm 1.2$ (mean $\pm$ SD, $n = 9$), is about half of that for ^{11}C-DASB ($10.1 \pm 2.0$, $n = 6$), suggesting low nonspecific binding as a likely explanation for favorably high BP. ^{11}C-MADAM seems to be the only member of this class for which convergence can be reached when applying a standard 3CM to PET data (2,36–38). Reaching convergence is a prerequisite for comparing the distribution volumes of the 3CM(1) and 3CM(2), thus providing support for the $BP_{Direct(2)}$ results. This validation has so far been presented only for ^{11}C-MADAM.

Rapid brain uptake is generally seen as advantageous for a radioligand and particularly advantageous for a peak or

**TABLE 5**
5-HTT Density in Human Brain in Vitro (pmol/g Tissue) (8–11) and In Vivo Using ^{11}C-MADAM (BP)

| Region | Laruelle et al. (11) saturation study | Bäckström et al. (8) saturation study | Plenge et al. (10) saturation study | Cortés et al. (9) autoradiography | Present study (SRTM, BP) PET |
| --- | --- | --- | --- | --- | --- |
| Frontal cortex | 5 | 6 | 5 | 37 | 0.6 |
| Cingulate cortex | 14 | 11 | 9 | — | 0.7 |
| Hippocampal complex | 14 | 7 | 7 | 42 | 1.2 |
| Putamen | 14 | 15 | 14 | 63 | 1.4 |
| Raphe nuclei | — | — | 82 | 200 | 4.0 |
| Cerebellum | 2 | 3 | — | 18 | — |

— = not applicable/not included.
Data are presented as mean values and are reprinted from (8–10) with permission from Elsevier and from (11) with permission from Society of Biological Psychiatry.
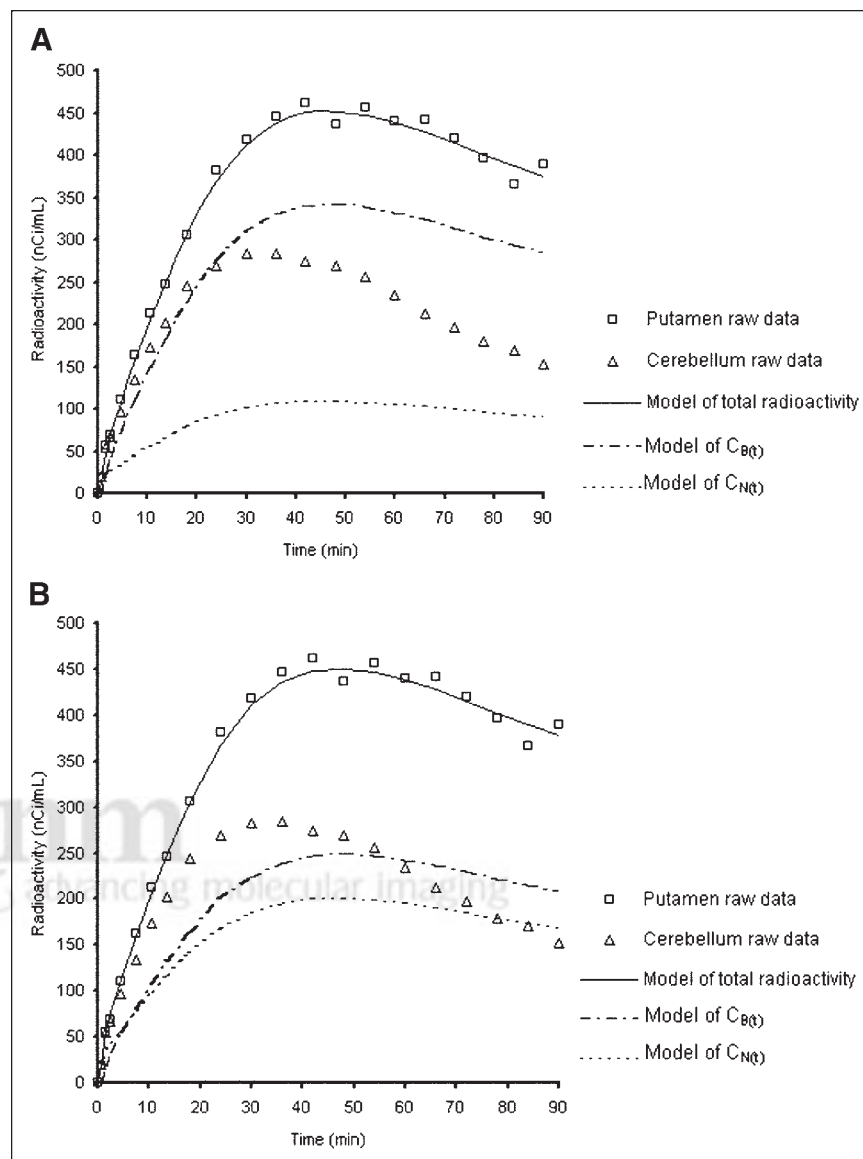
**FIGURE 7.** Experimental values for regional radioactivity in putamen and cerebellum presented together with calculated values of total radioactivity in putamen, specific binding, and free fraction according to 3CM(1) (A) and 3CM(2) (B).

**TABLE 6**
Time to Peak Uptake (Minutes) in 6 Regions for ^{11}C-MADAM ($n = 9$) and ^{11}C-DASB ($n = 6$) (39)

| | ^{11}C-MADAM | | | ^{11}C-DASB |
|---|---|---|---|---|
| Region | 3CM(1) | 3CM(2) | 2CM | 2CM |
| Raphe nuclei | $69.1 \pm 16.3$ | $70.1 \pm 17.1$ | $70.4 \pm 18.2$ | $71.3 \pm 18.6$ |
| Putamen | $35.6 \pm 6.1$* | $35.7 \pm 6.4$† | $36.0 \pm 6.6$† | $46.0 \pm 10.7$ |
| Hippocampal complex | $34.3 \pm 4.7$† | $34.3 \pm 5.1$† | $34.5 \pm 5.0$† | $42.5 \pm 8.8$ |
| Cingulate cortex | $30.8 \pm 6.0$ | $31.1 \pm 6.2$ | $31.0 \pm 6.2$ | $35.2 \pm 8.6$ |
| Frontal cortex‡ | $26.6 \pm 5.2$ | $26.8 \pm 5.4$ | $26.8 \pm 5.3$ | $29.4 \pm 6.9$ |
| Cerebellum | $24.2 \pm 5.0$ | na | $24.5 \pm 5.0$ | $29.3 \pm 8.5$ |

*$P < 0.1$ (comparison with ^{11}C-DASB data; 2-tailed $t$ test.
†$P < 0.05$.
‡[11]C-DASB data represent dorsolateral prefrontal cortex.
na = not applicable.
Data are presented as mean $\pm$ SD.

ratio analysis. ^{11}C-MADAM and ^{11}C-DASB both satisfy criteria for peak equilibrium—however, at a rather late time point after injection—when compared with established radioligands, such as ^{11}C-raclopride or ^{11}C-WAY 100635 (*16,34*). Of the 2 radioligands, ^{11}C-MADAM seems to reach equilibrium somewhat earlier than ^{11}C-DASB (Table 6).

## CONCLUSION

The regional binding distribution of ^{11}C-MADAM is consistent with postmortem data acquired with ^{3}H-MADAM (*6*) as well as the distribution demonstrated with other reference ligands in vitro (Table 5). The time–activity curves could be described by current major quantitative approaches, and the suitability of the cerebellum as a reference region for nonspecific ^{11}C-MADAM binding was confirmed, thus paving the way for simplified approaches advantageous for applied clinical studies, such as the SRTM.

## ACKNOWLEDGMENTS

## REFERENCES

1. Ohayon MM, Lader MH. Use of psychotropic medication in the general population of France, Germany, Italy, and the United Kingdom. *J Clin Psychiatry.* 2002;63:817–825.
2. Ginovart N, Wilson AA, Meyer JH, Hussey D, Houle S. Positron emission tomography quantification of [^{11}C]-DASB binding to the human serotonin transporter: modeling strategies. *J Cereb Blood Flow Metab.* 2001;21:1342–1353.
3. Meyer JH, Wilson AA, Sagrati S, et al. Serotonin transporter occupancy of five selective serotonin reuptake inhibitors at different doses: an [^{11}C]DASB positron emission tomography study. *Am J Psychiatry.* 2004;161:826–835.
4. Meyer JH, Wilson AA, Ginovart N, et al. Occupancy of serotonin transporters by paroxetine and citalopram during treatment of depression: a [^{11}C]DASB PET imaging study. *Am J Psychiatry.* 2001;158:1843–1849.
5. Larsen AK, Brennum LT, Egebjerg J, Sanchez C, Halldin C, Andersen PH. Selectivity of ^{3}H-MADAM binding to 5-hydroxytryptamine transporters in vitro and in vivo in mice: correlation with behavioural effects. *Br J Pharmacol.* 2004;141:1015–1023.
6. Chalon S, Tarkiainen J, Garreau L, et al. Pharmacological characterization of N,N-dimethyl-2-(2-amino-4-methylphenylthio)benzylamine as a ligand of the serotonin transporter with high affinity and selectivity. *J Pharmacol Exp Ther.* 2003;304:81–87.
7. Halldin C, Guilloteau D, Tarkiainen J, et al. [^{11}C]MADAM: a highly suitable radioligand for examination of the serotonin transporter with PET [abstract]. *Eur J Nucl Med.* 2001;28:973.
8. Backström I, Bergstrom M, Marcusson J. High affinity [^{3}H]paroxetine binding to serotonin uptake sites in human brain tissue. *Brain Res.* 1989;486:261–268.
9. Cortés R, Soriano E, Pazos A, Probst A, Palacios JM. Autoradiography of antidepressant binding sites in the human brain: localization using [^{3}H]imipramine and [^{3}H]paroxetine. *Neuroscience.* 1988;27:473–496.
10. Plenge P, Mellerup ET, Laursen H. Regional distribution of the serotonin transport complex in human brain, identified with ^{3}H-paroxetine, ^{3}H-citalopram and ^{3}H-imipramine. *Prog Neuropsychopharmacol Biol Psychiatry.* 1990;14:61–72.
11. Laruelle M, Vanisberg MA, Maloteaux JM. Regional and subcellular localization in human brain of [^{3}H]paroxetine binding, a marker of serotonin uptake sites. *Biol Psychiatry.* 1988;24:299–309.
12. Bergstrom M, Boethius J, Eriksson L, Greitz T, Ribbe T, Widen L. Head fixation device for reproducible position alignment in transmission CT and positron emission tomography. *J Comput Assist Tomogr.* 1981;5:136–141.
13. Tarkiainen J, Vercouillie J, Emond P, et al. Carbon-11 labelling of MADAM in two different positions: a highly selective PET radioligand for the serotonin transporter. *J Labelled Compds Radiopharm.* 2001;44:1013–1023.
14. Weinhard K, Dahlbom M, Eriksson L, et al. The ECAT EXACT HR: performance of a new high resolution positron scanner. *J Comput Assist Tomogr.* 1994;18:110–118.
15. Eriksson L, Holte S, Bohm C, Kesselberg M, Hovander B. Automated blood sampling systems for positron emission tomography. *IEEE Trans Nucl Sci.* 1988;35:703–707.
16. Farde L, Eriksson L, Blomquist G, Halldin C. Kinetic analysis of central [^{11}C]raclopride binding to D2-dopamine receptors studied by PET: a comparison to the equilibrium analysis. *J Cereb Blood Flow Metab.* 1989;9:696–708.
17. Halldin C, Swahn CG, Farde L, Sedvall G. Radioligand disposition and metabolism: key information in early drug development. In: Comer D, ed. *PET for Drug Development and Evaluation.* Dordrecht, The Netherlands: Kluwer Academic Publishers; 1995:55–65.
18. Roland PE, Eriksson L, Stone-Elander S, Widen L. Does mental activity change the oxidative metabolism of the brain? *J Neurosci.* 1987;7:2373–2389.
19. Koeppe RA, Holthoff VA, Frey KA, Kilbourn MR, Kuhl DE. Compartmental analysis of [^{11}C]flumazenil kinetics for the estimation of ligand transport rate and receptor distribution using positron emission tomography. *J Cereb Blood Flow Metab.* 1991;11:735–744.
20. Wong DF, Gjedde A, Wagner HN Jr. Quantification of neuroreceptors in the living human brain. I. Irreversible binding of ligands. *J Cereb Blood Flow Metab.* 1986;6:137–146.
21. Caceci MS, Cacheris WP. Fitting curves to data: the simplex algorithm is the answer. *Byte.* 1984;9:340–362.
22. Mintun MA, Raichle ME, Kilbourn MR, Wooten GF, Welch MJ. A quantitative model for the in vivo assessment of drug binding sites with positron emission tomography. *Ann Neurol.* 1984;15:217–227.
23. Lammertsma AA, Hume SP. Simplified reference tissue model for PET receptor studies. *Neuroimage.* 1996;4:153–158.
24. Logan J, Fowler JS, Volkow ND, et al. Graphical analysis of reversible radioligand binding from time-activity measurements applied to [N-11]C-methyl]-(-)-cocaine PET studies in human subjects. *J Cereb Blood Flow Metab.* 1990;10:740–747.
25. Ito H, Hietala J, Blomqvist G, Halldin C, Farde L. Comparison of the transient equilibrium and continuous infusion method for quantitative PET analysis of [^{11}C]raclopride binding. *J Cereb Blood Flow Metab.* 1998;18:941–950.
26. Olsson H, Farde L. Potentials and pitfalls using high affinity radioligands in PET and SPET determinations on regional drug induced D2 receptor occupancy: a simulation study based on experimental data. *Neuroimage.* 2001;14:936–945.
27. Halldin C, Lundberg J, Sóvágó J, et al. [^{11}C]MADAM, a new serotonin transporter radioligand characterised in the monkey brain by PET. *Synapse.* In press.
28. Akaike H. A new look at the statistical model identification. *IEEE Trans Automat Contr.* 1974;19:716–723.
29. Schwarz G. Estimating the dimension of a model. *Ann Stat.* 1978;6:461–564.
30. Cunningham VJ. Non-linear regression techniques in data analysis. *Med Inform (Lond).* 1985;10:137–142.
31. Suhara T, Sudo Y, Yoshida K, et al. Lung as reservoir for antidepressants in pharmacokinetic drug interactions. *Lancet.* 1998;351:332–335.
32. Lin K-J, Ye X-X, Yen T-C, et al. Biodistribution study of [^{123}I]ADAM in mice: correlation with whole body autoradiography. *Nucl Med Biol.* 2002;29:643–650.
33. Farde L, Hall H, Ehrin E, Sedvall G. Quantitative analysis of D2 dopamine receptor binding in the living human brain by PET. *Science.* 1986;231:258–261.
34. Farde L, Ito H, Swahn CG, Pike VW, Halldin C. Quantitative analyses of carbonyl-carbon-11-WAY-100635 binding to central 5-hydroxytryptamine-1A receptors in man. *J Nucl Med.* 1998;39:1965–1971.
35. Gunn RN, Gunn SR, Cunningham VJ. Positron emission tomography compartmental models. *J Cereb Blood Flow Metab.* 2001;21:635–652.
36. Huang Y, Hwang DR, Narendran R, et al. Comparative evaluation in nonhuman primates of five PET radiotracers for imaging the serotonin transporters: [^{11}C]McN 5652, [^{11}C]ADAM, [^{11}C]DASB, [^{11}C]DAPA, and [^{11}C]AFM. *J Cereb Blood Flow Metab.* 2002;22:1377–1398.
37. Zhu Z, Guo N, Narendran R, et al. The new PET imaging agent [^{11}C]AFE is a selective serotonin transporter ligand with fast brain uptake kinetics. *Nucl Med Biol.* 2004;31:983–994.
38. Huang Y, Narendran R, Bae SA, et al. A PET imaging agent with fast kinetics: synthesis and in vivo evaluation of the serotonin transporter ligand [^{11}C]2-[2-dimethylaminomethylphenylthio]-5-fluorophenylamine ([^{11}C]AFA). *Nucl Med Biol.* 2004;31:727–738.
39. Frankle WG, Huang Y, Hwang DR, et al. Comparative evaluation of serotonin transporter radioligands ^{11}C-DASB and ^{11}C-McN 5652 in healthy humans. *J Nucl Med.* 2004;45:682–694.

# Quantification of ^{11}C-MADAM Binding to the Serotonin Transporter in the Human Brain

Johan Lundberg, Ikuo Odano, Hans Olsson, Christer Halldin and Lars Farde

This article and updated information are available at:
**http://jnm.snmjournals.org/content/46/9/1505**

Information about reproducing figures, tables, or other portions of this article can be found online at:
**http://jnm.snmjournals.org/site/misc/permission.xhtml**

Information about subscriptions to JNM can be found at:
**http://jnm.snmjournals.org/site/subscriptions/online.xhtml**

SOCIETY OF
NUCLEAR MEDICINE
AND MOLECULAR IMAGING